INSTITUTE OF PHYSICS PUBLISHING NANOTECHNOLOGY
Nanotechnology **15** (2004) S190–S196 PII: S0957-4484(04)69814-X

Synthesis of acicular Fe–Co nanoparticles and the effect of Al addition on their magnetic properties

Raúl Pozas[1], Manuel Ocaña[1], M Puerto Morales[2], Pedro Tartaj[2], Nuria O Nuñez[2] and Carlos J Serna[2]

[1] Instituto de Ciencia de Materiales de Sevilla (CSIC-UNSE), Americo Vespucio s/n, Isla de la Cartuja, 41092 Sevilla, Spain
[2] Instituto de Ciencia de Materiales de Madrid (CSIC), Cantoblanco, 28049 Madrid, Spain

E-mail: mjurado@icmse.csic.es (Manuel Ocaña)

Received 26 September 2003
Published 9 February 2004
Online at stacks.iop.org/Nano/15/S190 (DOI: 10.1088/0957-4484/15/4/013)

Abstract
We have obtained Al(III)-protected Fe–Co metal nanoparticles with acicular shape by thermal reduction with hydrogen from Al(III)–Co(II)-codoped acicular goethite precursors prepared by oxidation with air of a $FeSO_4$ solution containing $Al(NO_3)_3$ and $Co(NO_3)_3$ precipitated with Na_2CO_3. These precursor particles were smaller (∼110 nm in length) than those prepared by a previously reported procedure, resulting in smaller metal particles (∼70 nm in length) suitable for high-density magnetic recording media in which higher bit-packing densities could be obtained. The location of Co and Al in the goethite precursors, as well as in the final metal particles, have been studied for a better understanding of role that these elements play in the microstructural features and the magnetic properties of the final metal particles. It was found that the Al content in the particle outer layers was enhanced during the reduction process, while cobalt diffuses toward the inner part of iron nanoparticles forming an Fe–Co alloy. The incorporation of cobalt helps to increase the magnetization saturation because it avoids corrosion and minimizes the growth of the iron crystals. The presence of Al(III) in the particle outer layers of the precursors inhibited the growth of iron crystals and preserved the acicular shape during the reduction process, which has a very favourable effect on the coercivity and the squareness of the metal samples.

1. Introduction

Recently, with the development of high saturation magnetization pigments with high coercivities in the nanometre size range, the use of advanced metal pigments (MP) in flexible technology has expanded dramatically [1–3]. These particulate media consist of Fe-based acicular particles deposited longitudinally on a film [4–6]. Acicular particles are preferred over equiaxial ones due to their higher shape anisotropy. In addition, due to the need to improve bit-packing densities, small particle sizes (above the superparamagnetic size limit) are required for high-density recording media. Thus, new magnetic FePt nanoparticles with sizes in the 3–5 nm range, have recently been suggested as promising candidates for future high density magnetic storage technology [7].

The only commercially significant process for the production of iron metal acicular particles is the thermal reduction with hydrogen of acicular α-FeOOH (goethite) particles [8–10]. Elements such as Al, B, Si, P and Sn are usually added to the system to increase their corrosion resistance and to protect the particles against sintering during thermal heating [4–6].

The presence of cobalt in the MP is very important to improve the magnetic properties of iron. It is well known from the Slater–Pauling curve that the addition of cobalt up to 30 mol% increases the magnetization of iron [11],

which leads to an increase in the magnitude of saturation magnetization. Moreover, the presence of Co improves the corrosion resistance, probably due to the formation of a Co–ferrite layer on the surface of the particles which helps to minimize the progress of oxidation, and which is especially important for the smallest particles required for high-density recording media [8, 12]. Furthermore, there is some indication that the addition of cobalt yields particles having smoother surfaces [13] in which the number of nucleation sites where magnetization reversal is initiated are reduced, further increasing coercivity. In summary, the addition of cobalt is essential to increase coercivity and saturation magnetization, although the precise role of cobalt in improving the magnetic characteristics of the metal particles still remains unclear.

Several studies have been carried out on the synthesis of Fe–Co MP from Co(II) adsorbed onto acicular goethite precursors [12, 14, 15]. However, this process involves the use of high temperatures (∼700 °C) to diffuse the Co toward the inner part of iron particles, leading to sintering between particles and the particles losing their acicular shape. In this sense, it would be highly desirable for Co-doped precursors having uniform distribution of sizes and high chemical homogeneity to be available [16]. With this purpose, we have recently shown that the thermal reduction of goethite precursors prepared by a modified carbonate route, that essentially consists in a two-step method, in which NaOH and Na_2CO_3 are used as precipitating agents, produces Fe-based alloys with adequate microstructure and good magnetic properties [16–18]. However, the average particle size obtained (about 120 nm) was somewhat larger than those used in the most advanced MP today.

The aim of this work is the preparation of acicular Co–Fe alloys consisting of acicular nanoparticles with a reduced size with respect to those previously reported [16], so that bit-packing density could be increased. They were prepared by thermal reduction with H_2 of Co–goethite precursors obtained by using a method previously reported which only used Na_2CO_3 as a precipitating agent in a single step [19]. The Co-doped goethite precursors were also protected with Al(III) cations, since it has recently been shown that these cations may successfully protect the most advanced metal particulate recording media against sintering [8]. It should be noted that in our previous work on the larger Fe–Co particles [16], the Al(III) cations were added by coating the preformed Co-doped goethite precursors, whereas in this study they were incorporated by doping during their synthesis process. The Co–goethite particles so-obtained were characterized in terms of their morphology, composition and crystalline structure, in order to determine the location of both cobalt and aluminium ions in the particles. Finally, the magnetic properties of the alloys obtained were evaluated and the effect of both elements (Al and Co) on the microstructural features and the magnetic properties of the final MP were also discussed.

2. Experimental details

2.1. Preparation of the precursors

For the preparation of the acicular Al(III)–Co(II)-doped goethite particles (named as sample G_{CoAl}), 0.6 mol dm^{-3} aqueous solutions of Fe(II) sulphate ($FeSO_4{\cdot}7H_2O$, Aldrich, 99%) containing appropriated amounts of Co(II) nitrate ($Co(NO_3)_2{\cdot}6H_2O$, Aldrich 98%) and Al(III) nitrate ($Al(NO_3)_3{\cdot}9H_2O$, Fluka, 99%) were first precipitated by the addition of an 0.9 mol dm^{-3} aqueous solution of sodium carbonate (Na_2CO_3, Aldrich 99.5%) and the resulting dispersions were then oxidized at constant temperature (40 °C) for 6 h by bubbling air at a constant flow rate (2 dm^3 min^{-1}) following the method described earlier for the preparation of undoped goethite particles [19]. In addition, we also used this procedure to prepare both pure goethite (named as G) and Co(II)-doped goethite (named as G_{Co}) samples for comparison purposes.

In all cases, after oxidation, the resulting precipitates were cooled, centrifuged and washed several times with de-ionized water for purification. Finally, the powdered solids were collected by filtration and dried at 50 °C before analyses.

2.2. Thermal reduction

To obtain the final metal particles, the goethite samples (∼60 mg) were first heated for 4 h in air for dehydroxylation yielding hematite (α-Fe_2O_3) which was then reduced, at constant temperature, in a hydrogen (99.9999%) stream (flow rate = 20 l h^{-1}) for 4 h [20]. The samples were then cooled down to room temperature, under the hydrogen atmosphere and, finally, passivated by exposing them for 1 h to alcohol vapours, which were generated by bubbling N_2 gas (99.999%) at constant flow rate (40 l h^{-1}) into a flask containing pure (99.8%) ethanol. Samples prepared after reduction of G, G_{Co} and G_{CoAl} precursors are named as Fe, Fe_{Co} and Fe_{CoAl} respectively. Dehydroxylation and reduction temperatures were optimized in each case to get the complete reduction and minimize the loss of acicular morphology of the particles.

2.3. Characterization techniques

Transmission electron microscopy (TEM, Philips 200 CM) was used to examine the morphology of the particles. The particle size distribution of the powders was evaluated from the electron micrographs by counting around one hundred particles. From these data, the degree of polydispersity, defined as the standard deviation (SD)/mean size [21], was evaluated. The mean and the SD values associated with the axial ratio (L/W) were determined from the L/W ratios obtained for each particle.

Phase identification was carried out by x-ray diffraction (XRD) in a Siemens D501 apparatus using Cu Kα radiation and a diffracted beam graphite monochromator. An estimation of the crystallite size was determined from the full width at half maximum of the XRD selected reflection by using the Scherrer equation [22]. Differential thermal (DTA) and thermogravimetric (TGA) analyses (Seiko, EXSTAR 6000) were carried out in air at a heating rate of 10 °C min^{-1}.

The quantitative composition of the samples in terms of the Al, Co and Fe contents was determined by x-ray fluorescence (XRF, Siemens SRS 3000). Energy dispersive x-ray analysis (EDX, Philips DX4), installed in the TEM microscope, was also used to gain information on the particle composition. The variation of the aluminium and cobalt concentrations in the particle outer layers during the transformation from goethite to hematite and finally to iron was analysed from the XPS

spectra, recorded in a VG Escalab 220 using the Mg Kα excitation source. Calibration of the binding energy scale of the spectra was done at the C 1s peak of the surface carbon contamination taken at 284.6 eV. Atomic percentages of the elements were calculated from the peak areas after background subtraction (Shirley background). The areas were referred to the sensitivity factors of the elements as supplied by the instrument manufactures.

Temperature programmed reduction (TPR) experiments were performed in a conventional apparatus connected to a computer for data storing and processing, using a thermal conductivity detector (TCD), calibrated using different amounts of CuO as previously described [23]. The reactive gas (5% H_2 in Ar, flow rate = 50 cm^3 min^{-1}) was passed through 5 mg of sample, which was heated up to 600 °C at a constant heating rate of 5 °C min^{-1}.

Magnetic characterization of the samples was carried out in a vibrating sample magnetometer (MLVSM9 MagLab 9 T, Oxford Instrument). Magnetization curves were recorded at room temperature by first saturating the sample in a field of 3 T. Then, the saturation magnetization (M_s), the squareness (M_r/M_s, where M_r is the remanent magnetization) and the coercivity (H_c) were determined for each sample. The M_s values were evaluated by extrapolating to infinite field the experimental results obtained in the high field range where the magnetization linearly increase with $1/H$.

3. Results and discussion

3.1. Goethite precursors

The obtained undoped goethite particles (figure 1) showed a length of 200 nm (sample G) and an axial ratio of 5 (table 1). Under the same experimental conditions, used for this sample, the maximum cobalt amount (Co/Fe + Co mole ratio) that could be incorporated to the goethite precursor corresponded to ∼10%. For higher Co contents, the appearance of both secondary phases and irregular particles were observed. The addition of cobalt up to this limiting value yielded single phase goethite particles (figure 1) with a similar degree of acicularity, although with smaller particle size (120 nm) and broader size distribution (table 1). These precursor particles were also smaller than those with similar composition previously prepared by the double step procedure [16].

The cobalt content measured by XRF was similar to the nominal value, suggesting the complete precipitation of cations. Chemical analyses carried out on single particles by EDX also showed a similar composition to that of the overall solid, which manifests a good chemical homogeneity at particle level. However, the molar percentage of cobalt obtained from XPS measurements, was higher (25 mol%) than the overall value (10 mol%), indicating an enrichment in cobalt in the outer layers of the goethite particles. Crystal sizes obtained from the (020) XRD reflection of goethite for the G_{Co} sample (∼27 nm) (table 1) were similar to the particle width observed by TEM, suggesting the single crystal character of the particles and that the (001) crystallographic axis is along the longest particle dimension, in accordance with the crystal habit of growth for this solid [24]. Such structural features were confirmed in our previous work for undoped goethite particles from high-resolution TEM and electron diffraction [19].

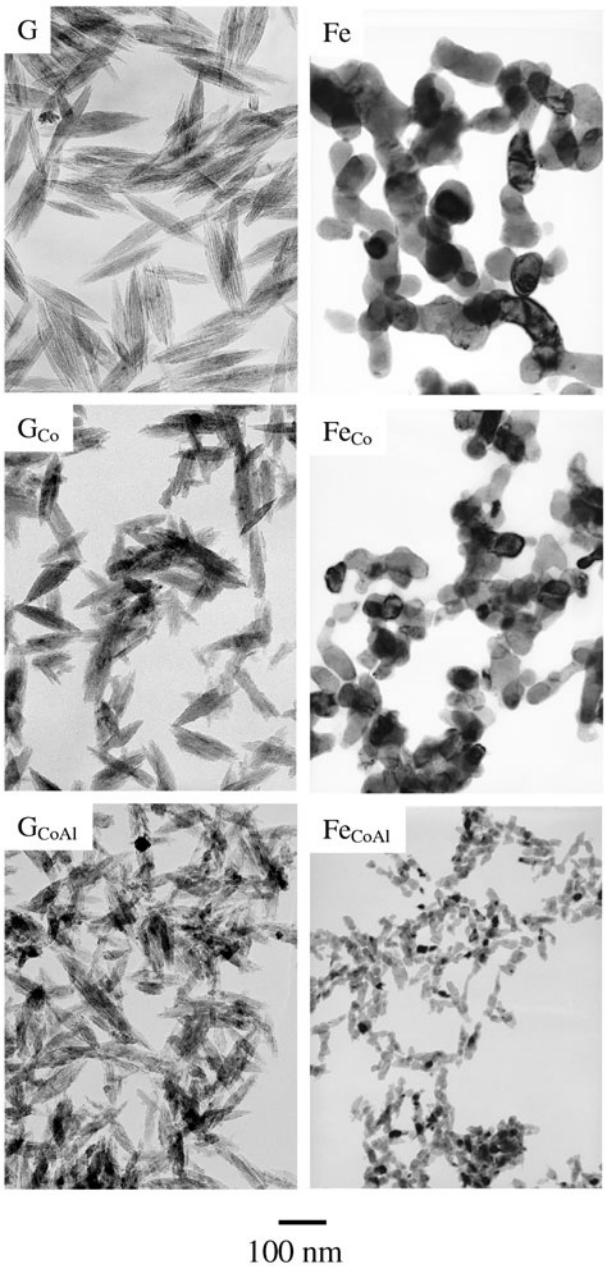

Figure 1. Goethite particles synthesized in the absence (G) and the presence of cobalt (G_{Co}) or cobalt and aluminium cations (G_{CoAl}) and their corresponding iron nanoparticles (Fe, Fe_{Co} and Fe_{CoAl}).

Under the conditions described in the experimental section and keeping the maximum molar percentage of cobalt (10%) used to obtain uniform Co-doped goethite particles, the maximum aluminium amount (Al/Fe + Co + Al mol ratio) that could be incorporated to these precursors was about 5%, since for higher values rounded particles were detected. This maximum amount of Al decreased the particle size (107 nm × 26 nm) in relation to that of the sample obtained in the absence of Al(III) (sample G_{Co}) (120 nm × 27 nm), but it does not affect both degree of acicularity (axial ratio ∼5) (figure 1) and crystalline structure, which consisted of single phase goethite (table 1). Furthermore, the presence of aluminium cations gave rise to a sharper particle size distribution (a decrease in the

Table 1. Morphological characteristics (shape, length, width, axial ratio) and crystal size measured from the (012) x-ray reflection for the goethite samples (the relative standard deviations are included in parenthesis).

Sample	Co/(Fe + Co + Al) (mol%)	Al/(Al + Co + Fe) (mol%)	Length (nm)	Width (nm)	Axial ratio	Crystal size (nm)
G	—	—	200 (20)	43 (32)	5.0 (29)	40
G_{Co}	10	—	120 (35)	27 (39)	4.7 (38)	27
G_{CoAl}	10	5	107 (27)	26 (31)	4.5 (25)	27

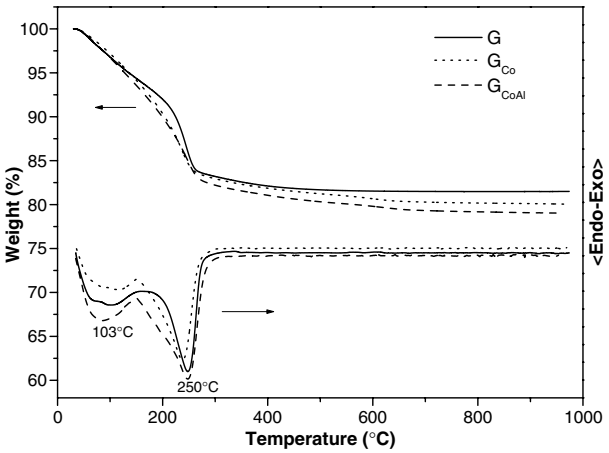

Figure 2. TG and DTA analyses for goethite (G) Co-doped goethite (G_{Co}) and Al–Co–codoped goethite (G_{CoAl}) samples.

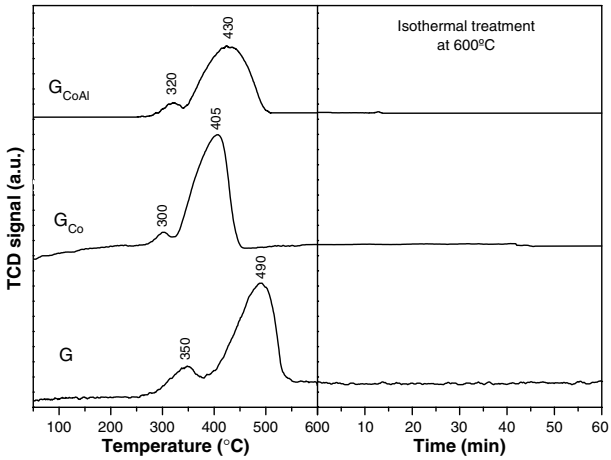

Figure 3. TPR profiles for G, G_{Co} and G_{CoAl} samples previously heated at 300 °C.

polydispersity degree from 35% to 27% in the long dimension was observed for the G_{CoAl} sample (table 1)).

XRF analyses of the G_{CoAl} sample showed that the Al and Co contents were similar to the nominal value, while EDX analyses indicated a homogeneous distribution of both elements in each particle. In addition, both ions were found in higher proportion in the particle outer layers (29 mol% for Co and 9 mol% for Al cations) in relation to the amount observed by XRF (10%), indicating an enrichment in both elements in the outer layers of the precursor particles. As in the case of sample G_{Co}, the crystal size measured from (020) reflection of goethite for the G_{CoAl} sample (∼27 nm) was similar to the particle width measured (table 1), also suggesting a single crystal character of the particles and that the (001) crystallographic axis is along the longest particle dimension.

3.2. Preparation of iron metal particles

The goethite particles were transformed to metal iron in two steps aiming to reduce internal porosity and avoid further alterations of the particle morphology. Thus, they were first dehydroxylated to hematite which was then reduced to iron. The dehydroxylation process was studied by DTA/TG analyses (figure 2). As observed, the thermal behaviour of all goethite particles was similar, showing a broad endothermic peak below 165 °C due to the release of adsorbed water and a strong endothermic peak at ∼250 °C which is related to the goethite dehydroxylation to give hematite (α-Fe_2O_3) [25]. On this basis, the goethite–hematite transformation was carried out by heating the samples at 300 °C at which temperature the particle morphology remained unaffected.

The acicular hematite particles so-obtained were then reduced in the presence of H_2 at a temperature which was also optimized in order to minimize the possible particle sintering during this treatment. For this purpose, temperature programmed reduction (TPR) experiments were carried out. The TPR profile of the hematite obtained from the undoped goethite sample (figure 3) clearly showed that the reduction process took place under non-isothermal conditions, from 250 to 550 °C in two well-resolved reduction steps. The hydrogen uptakes obtained by numerical integration of the peak areas indicated that the first step (∼350 °C) was due to the transformation of hematite to magnetite (Fe_3O_4), whereas the second one (∼490 °C), was due to the reduction of magnetite to metal iron. It should be noted that the position of these two maxima was considerably higher for the hematite particles obtained from undoped goethite (sample G) than for Co-doped goethite (sample G_{Co}) (300 and 405 °C respectively) (figure 3), which suggested that the presence of cobalt cations in the hematite precursor clearly accelerates its reduction process. However, an opposite effect was observed for the sample containing aluminium (sample G_{CoAl}) for which such peaks appeared at 320 and 430 °C respectively (figure 3), indicating that the aluminium cations retard the reduction process, in agreement with previous observations for Al-doped goethite [18]. It seems that the presence of Al(III) ions at the particle surface hampers the transport of water, needing higher reduction temperatures for its total release, as previously suggested [26].

In view of these results, the hematite samples were reduced under the isothermal conditions described in the experimental section, at increasing temperatures starting from 300 °C, finding that the minimum temperature required to complete reduction of these samples, was 325 °C, as indicated by x-ray diffraction, which only showed the α-Fe peaks in all cases (figure 4). These samples were selected for the

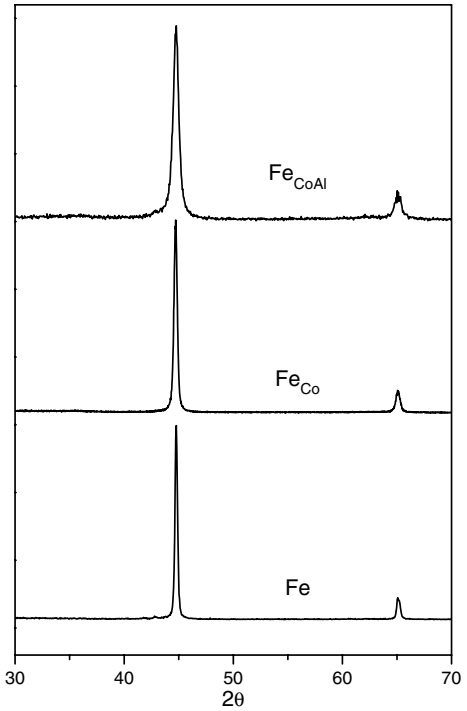

Figure 4. X-ray diffraction patterns obtained for Fe, Fe–Co alloy (Fe_{Co}) and Al-protected Fe–Co alloy (Fe_{CoAl}) samples after thermal reduction at 325 °C for 4 h.

Table 2. Magnetic properties (M_s = saturation magnetization, H_c = coercivity, M_r = remanent magnetization and M_r/M_s = squareness) and crystal size obtained for iron, Fe–Co alloy (Fe_{Co}) and Al-protected Fe–Co alloy (Fe_{CoAl}) samples obtained from the corresponding goethite precursors.

Sample	Crystal size (nm)	H_c (Oe)	M_s (emu g^{-1})	M_r/M_s
Fe	123	450	179	0.23
Fe_{Co}	58	650	217	0.34
Fe_{CoAl}	23	1070	131	0.47

evaluation of their magnetic properties since at this temperature the acicular morphology losses during the reduction process are minimized.

It should be noted that the crystal size measured from the (100) x-ray reflection peak of α-Fe increased for Fe and Fe_{Co} samples (123 and 58 nm respectively) (table 2) in relation to those observed for the shorter dimension of their corresponding precursors (40 and 27 nm, respectively) (table 1), suggesting the presence of interparticle sintering, which was less important for the particles containing cobalt. However, this effect was not observed for the sample containing Al (sample Fe_{CoAl}), for which the crystal size was even slightly lower (23 nm) (table 2) than that for the G_{CoAl} precursor (27 nm) (table 1), suggesting that the presence of Al cations in the precursor particles minimizes the growth of iron crystal during the thermal reduction process.

In addition, TEM micrographs of Fe and Fe_{Co} particles (figure 1) showed a clear loss of acicular shape as a consequence of sintering during thermal reduction, in accordance with the higher crystal size measured for both samples (table 2). However, the Fe_{CoAl} particles kept the acicular morphology of the corresponding precursor (G_{CoAl} sample) (figure 1) resulting in metal particles of ∼70 nm length which are much smaller than those prepared from Co-doped goethite particles obtained by a double-step procedure further coated with Al(III) hydroxide (120 nm) [16]. This size reduction makes our samples interesting for high-density magnetic recording media since higher bit-packing densities could be obtained. The lack of sintering associated with the Al addition can be understood in view of the variation of the aluminium concentration in the particle outer layers of the Al–Co–goethite sample during its transformation to hematite and then to metal iron followed by XPS measurements (figure 5). Thus, the Al/Fe + Co + Al mole ratio increased from 8% for the G_{CoAl} sample to 33% for sample Fe_{CoAl} (figure 5), indicating a further and more important enrichment of Al cations in the particle outer layers during its reduction process, which explains its role in avoiding interparticle sintering. In addition, it was observed that the proportion of cobalt in the particle outer layers decreased from goethite to iron for both Fe_{Co} and Fe_{CoAl} samples, respectively (figure 5), which suggested the diffusion of this cation to the inner part of the iron particles and, thereby, the formation of Fe–Co alloy, as previously observed by other authors [14, 15].

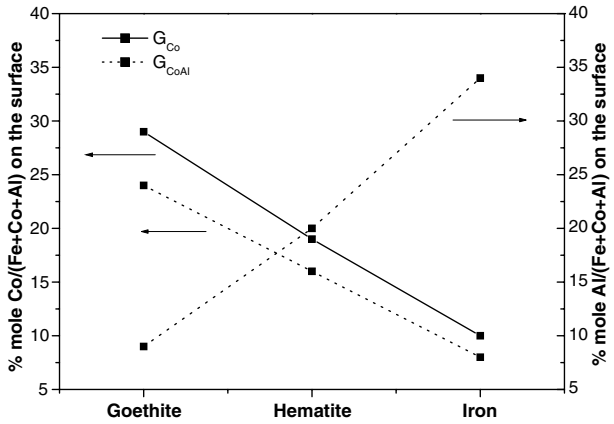

Figure 5. Variation of the aluminium and cobalt concentration evaluated from the XPS spectra during the transformation from goethite to hematite and finally to metal iron for G_{Co} and G_{CoAl} samples.

Finally, the position observed for the Fe $2p_{3/2}$ (710.3 eV) and Co $2p_{3/2}$ (780.3 eV) XPS peaks (data not shown) was consistent with the presence of oxidized iron and cobalt in the particle outer layers, which could consist of a ferrimagnetic spinel phase similar to that suggested for Al-doped iron from Mössbauer studies [18].

3.3. Magnetic properties of iron particles

The magnetic parameters obtained from the hysteresis loops represented in figure 6 are summarized in table 2. All values obtained for saturation magnetization (M_s) were lower than expected for bulk Fe (∼220 emu g^{-1}) and Fe–Co (∼230 emu g^{-1} for a 10% Co content) [27], due to the presence of the oxide passivating layer on the particle surface [16, 18]. The largest M_s values obtained for both Fe and Fe_{Co} samples, when compared with the sample containing aluminium (Fe_{CoAl}), can be explained by the presence of a non-magnetic Al oxide in the particle outer layers of the

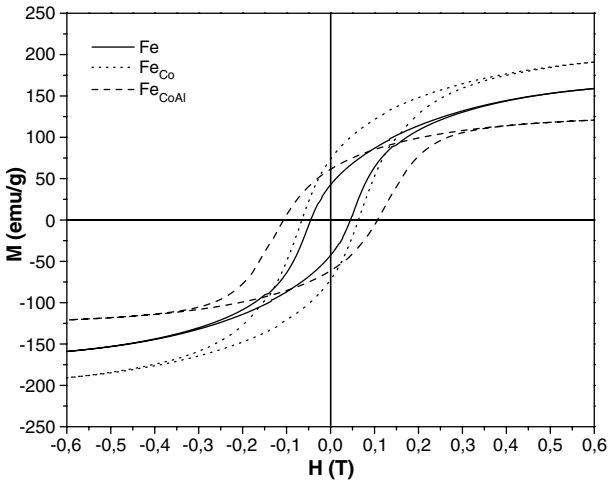

Figure 6. Section between −0.6 and 0.6 T of the magnetization curves obtained at room temperature for the Fe, Fe–Co alloy (Fe_{Co}) and Al-protected Fe–Co alloy (Fe_{CoAl}) samples.

latter and the higher size of the former samples (due to the sintering process), which therefore present a lower thickness for the passivation oxide layer. The higher M_s value for sample Fe_{Co} when compared with sample Fe, in spite of the larger crystal size of the latter, has been attributed to both the high magnetization of Fe–Co alloy and the probable thinner oxide layer formed on the particle surface [12]. This assumption was confirmed by the estimation of the iron oxide content of the particles in both samples. For Fe and FeCo metal particles of about these sizes we can expect values of M_s similar to those of the bulk [15, 16]. Thus, by taking into consideration the M_s value for bulk Fe (220 emu g^{-1}) and Fe–Co intermetallic alloy (230 emu g^{-1}) and a value of 10–20 emu g^{-1} for the iron oxide spinel (assumed to be nanocrystals of maghemite of about 2 nm) [28, 29], an iron oxide content of about 20% for sample Fe and 10% for sample Fe–Co resulted. Therefore, the particles containing cobalt showed superior corrosion resistance compared with those that were undoped as previously suggested [12]. It should be noted that the increase in the squareness (M_r/M_s) values from 0.23 and 0.34 for Fe and Fe_{Co} samples to 0.47 for the Fe_{CoAl} sample (table 2) suggests that the magnetization reversal changes from a more multidomain mechanism for Al-free samples, to a more monodomain mechanism for the Al-protected sample due to the decrease in crystal size [15].

The incorporation of Co also has a positive effect on the increase in coercivity (H_c) of metal samples. Thus, the coercivity value increased from 450 Oe for sample Fe to 650 Oe for sample Fe_{Co} (table 2). The role that cobalt plays in this coercivity increase must be ascribed to the increase of magnetic anisotropy [27] but it also seems to be correlated with the smaller crystal size observed for the Fe–Co alloy with respect to pure Fe (from 123 to 58 nm), since it favours a magnetic single domain behaviour [15]. This smaller size is in part due to the smaller particle size of the G_{Co} precursor and also to a possible weak effect of cobalt to avoid interparticle sintering. However, a more important increase in coercivity (from 650 to 1070 Oe) was found for the Al-protected sample. This behaviour is clearly associated with the preservation of the acicular particle shape during reduction associated with the presence of aluminium, since it is well known that the main factor that contributes to an increase in the coercivity values is shape anisotropy.

4. Conclusions

The use of a single-step carbonate route instead of a previously reported two-step carbonate route (NaOH plus Na_2CO_3 as precipitation agent) for the production of goethite precursors, has allowed us to obtain acicular Fe–Co metal nanoparticles protected by Al addition with smaller sizes (70 nm versus 120 nm in length), which in principle could be more adequate for high-density recording applications. Moreover, we have been able to explain the role that Co and Al play in improving the magnetic behaviour of the final metal particles. Thus, we have found that the incorporation of cobalt helps to increase the magnetization saturation not only because the magnetization is higher for the Fe–Co alloy, but also because it minimizes corrosion and the growth of the iron crystals, which also has a favourable effect on the squareness and the coercivity of the metal samples. Finally, we have also shown that the presence of Al is essential in preserving the acicular shape (high shape anisotropy values) of the particles. The beneficial effect of Al added by doping has been associated with the enrichment in this element of the outer layer of the metal particles.

Acknowledgments

This work was supported by the Spanish CICYT under projects MAT2002-04001-C02 and MAT2003-01479. The fellowships of Raúl Pozas and Nuria O Nuñez from the Spanish Ministerio de Ciencia y Tecnología and the Agencia Española de Cooperación Iberoamericana, respectively, are gratefully acknowledged. Pedro Tartaj acknowledges the financial support of the Ramon y Cajal project.

References

[1] Bates G 1991 *J. Magn. Magn. Mater.* **100** 413
[2] O'Grady K, White R L and Grundy P J 1998 *J. Magn. Magn. Mater.* **177** 886
[3] O'Grady K and Laidler H 1999 *J. Magn. Magn. Mater.* **200** 616
[4] Sharrock M P 2000 *IEEE Trans. Magn.* **36** 2420
[5] Morales M P, Walton S A, Prichard L S, Serna C J, Dickson D P E and O'Grady K 1998 *J. Magn. Magn. Mater.* **190** 357
[6] Onodera S, Kondo H and Kawana T 1996 *Mater. Res. Soc. Bull.* (Sept.) 35
[7] Zeng H, Sun S, Sandstrom R L and Murray C B 2003 *J. Magn. Magn. Mater.* **266** 227
[8] Hisano S and Saito K 1998 *J. Magn. Magn. Mater.* **190** 371
[9] Hisano S, Saito K, Aizawa S, Sano K, Matsumoto K and Murata K 1996 Ferromagnetic metal powder *US Patent Specification* no 5534361
[10] Hisano S, Saito K, Aizawa S, Sano K, Matsumoto K and Murata K 1997 Ferromagnetic metal powder *US Patent Specification* no 5591535
[11] Bozorth R M 1951 *Ferromagnetism* (New York: Van Nostrand-Reinhold) p 441
[12] Kisimoto M, Nakazumi T, Otani N and Sueyoshi T 1991 *IEEE Trans. Magn.* **27** 4645
[13] Okamoto K, Okazaki Y, Nagai N and Uedaira S 1996 *J. Magn. Magn. Mater.* **155** 60
[14] Kawasaki M and Higuchi S 1972 *IEEE Trans. Magn.* (Sept.) 430

[15] Sueyoshi K, Tashita K, Hirai S, Kisimoto M, Hayashi Y and Amemiya M 1982 *J. Appl. Phys.* **53** 2570
[16] Nuñez N O, Tartaj P, Morales M P, Pozas R, Ocaña M and Serna C J 2003 *Chem. Mater.* **15** 3558
[17] Nuñez N O, Morales M P, Tartaj P and Serna C J 2000 *J. Mater. Chem.* **10** 2561
[18] Nuñez N O, Pozas R, Morales M P, Tartaj P, Bonville P, González-Elipe A R, Caballero A, Ocaña M and Serna C J 2003 *Chem. Mater.* **15** 951
[19] Pozas R, Morales M P, Ocaña M and Serna C J 2002 *J. Colloid Interface Sci.* **254** 87
[20] Varanda L C, Jafelicci M Jr, Tartaj P, González-Carreño T, Morales M P, Muños T, Serna C J and O'Grady K 2002 *J. Appl. Phys.* **92** 2079
[21] Hunter R 1987 *Foundations of Colloid Science* (Oxford: Clarendon) p 127
[22] Azároff L V 1968 *Elements of X-ray Crystallography* (New York: McGraw-Hill) p 549
[23] Malet P, Munuera G and Caballero A 1989 *J. Catal.* **115** 567
[24] Cornell R M, Mann S and Skarnulis J 1983 *J. Chem. Soc. Faraday Trans.* **79** 2679
[25] Fey M V and Dixon J B 1981 *Clays Clay Miner.* **29** 91
[26] Van Der Giessen A A and Klomp C J 1969 *IEEE Trans. Magn.* **5** 317
[27] Cullity B D 1972 *Introduction to Magnetic Materials* (Reading, MA: Addison-Wesley)
[28] Morales M P, Veintemillas-Verdaguer S, Montero M, Serna C J, Roig A, Casas Ll, Martínez B and Sadiumenge F 1999 *Chem. Mater.* **11** 3058
[29] Tartaj P, González-Carreño T and Serna C J 2001 *Adv. Mater.* **13** 1620